MUSTA: A MULTI-STAGE NUMERICAL FLUX

E. F. Toro

Laboratory of Applied Mathematics
Faculty of Engineering, University of Trento
Trento, Italy
E-mail: toro@ing.unitn.it
Website: http://www.ing.unitn.it/toro

Abstract. Numerical methods for conservation laws constructed in the framework of finite volume and discontinuous Galerkin finite elements require, as the building block, a monotone numerical flux. In this paper we present a **MUlti-STAge** approach, called **MUSTA**, for constructing *upwind* numerical fluxes. The scheme may be interpreted as an *un-conventional approximate Riemann solver* that has simplicity and generality as its main features. When used in its first-order mode the scheme achieves the accuracy of *the best of the first-order upwind schemes*, the Godunov method used in conjunction with the exact Riemann solver. This is the reference first-order method for hyperbolic systems. Extensions of the scheme are realized in the framework of existing approaches. Here we present a second-order TVD scheme for three-dimensional non-linear systems and show numerical results for the two-dimensional Euler equations on non-Cartesian geometries. The schemes find their best justification when solving very complex systems for which the solution of the Riemann problem, in the classical sense, is too complex, too costly or is simply unavailable.

1 Introduction

Numerical methods for solving non-linear systems of hyperbolic conservation laws via finite volume methods or discontinuous Galerkin finite element methods require, as the building block, a monotone numerical flux. The choice of the building block has a profound influence on the properties of the resulting schemes. There are essentially two approaches for providing a monotone numerical flux. The simplest approach utilizes a symmetric stencil and does not explicitly make use of wave propagation information in the construction of the numerical flux. This approach gives rise to *centred* or *symmetric* schemes [15], [10], [18], [40], [28], [17], [30], [2]. A more refined approach utilizes wave propagation information contained in the differential equations to construct the numerical flux. This is done through the exact or approximate solution of the Riemann problem. Due to the fact that wave propagation information is used, these methods are called *upwind* methods or *Godunov-type methods* [5], [9], [6], [37], [20], [4], [27]. For up-to-date background on these methods see [16], [8], [14], [29], [35], [1].

Within the class of existing monotone first-order fluxes, the first-order upwind scheme of Godunov is the best, it has the smallest local truncation error. However, the superior accuracy of upwind methods comes at a cost, one must solve exactly or approximately, the Riemann problem. Conventional approximate Riemann solvers are usually complex and are not available for many systems of practical insterest, such as for models for compressible multi-phase flows. It would desirable to construct a numerical flux that emulates the best flux available but has simplicity and generality.

In this paper we present an approach that closely approximates the above aspirations. The computation of a numerical flux is carried out via a multi-stage predictor-corrector procedure,

using a *simple* numerical flux at each stage. In essence, our multi-stage approach may be regarded as an approximate Riemann solver in which the predictor stage *opens the Riemann fan* without making use of knowledge of the structure of the solution of the Riemann problem. In addition, the information extracted from the *opened* Riemann fan is precisely the information required for the evaluation of the intercell numerical flux sought; there is no logic associated with the complex solution-sampling procedure that is necessary when using an exact Riemann solver. The simpler sampling logic of conventional approximate Riemann solvers is also absent in our approach. Our method finds its best justification for complex systems of conservation laws such as those in compressible multi-phase fluid dynamics and magnetohydrodynamics.

The flux can then be used as the building block for constructing schemes of higher order of accuracy following existing methodologies, such as TVD methods [11], [30]; ENO/WENO methods [13], [12], [22]; ADER methods [31], [33], [25],[21], [24] and discontinuous Galerkin finite element methods [3], [36]. We remark that in higher-order schemes the difference in accuracy at the level of the first-order flux used, although less obvious, does persist, particularly for linearly degenerate fields and for long-time evolution problems [34]. Partial, preliminary results of the MUSTA flux are found in [26].

The rest of this paper is organized as follows. In section 2 we review existing numerical fluxes relevant to this paper. In section 3 we present our multi-stage predictor-corrector approach and discuss extensions. In section 4 we show some numerical results for the compressible Euler equations in one and two space dimensions on non-Cartesian geometries. Conclusions are drawn in section 5.

2 Monotone Schemes

Finite volume and discontinuous Galerkin finite element methods rely on a monotone, first-order intercell numerical flux, the building block of the schemes. Here we briefly review existing numerical fluxes in the frame of the finite volume approach.

2.1 The Finite Volume Framework

For our purpose it is sufficient to consider a general time-dependent non-linear system of hyperbolic conservation laws in two space dimensions

$$\partial_t \mathbf{Q} + \partial_x \mathbf{F}\left(\mathbf{Q}\right) + \partial_y \mathbf{G}\left(\mathbf{Q}\right) = \mathbf{0} \ , \tag{1}$$

in which $\mathbf{Q}$ is the vector of conserved variables and $\mathbf{F} = \mathbf{F}(\mathbf{Q})$ and $\mathbf{G} = \mathbf{G}(\mathbf{Q})$ are the vectors of fluxes in the Cartesian coordinate directions x and y respectively. In the presence of discontinuous solutions one uses the integral form of (1), which is obtained, for example, by integrating (1) on a control volume V, leading to

$$\frac{d}{dt} \int \int_V \mathbf{Q} \, dV = - \int_A (\mathbf{F}, \mathbf{G}) \cdot \mathbf{n} dA \ . \tag{2}$$

Here A is the boundary of the control volume V and $\mathbf{n}$ is unit vector pointing in the outward direction normal to the boundary A. In the finite volume approach one does not require a change of coordinates, such as body-fitted coordinates, to deal with domains whose boundaries are not aligned with the Cartesian directions; discretisation is performed directly in physical space. Assuming the domain of interest has been discretised by an appropriate mesh, we then

apply (2) to a finite volume or cell V_i to construct numerical schemes. In particular, a fully discrete finite volume scheme reads:

$$\mathbf{Q}_i^{n+1} = \mathbf{Q}_i^n - \frac{\Delta t}{\Delta V_i} \sum_{s=1}^{s=N} L_s \mathbf{T}_s^{-1} \mathbf{F}_{(i,s)} \ . \tag{3}$$

Here $\mathbf{Q}_i^n$ is the integral average of $\mathbf{Q}$ in volume V_i at time level n, N is the total number of faces of V_i, L_s is the length of face s, $\mathbf{T}_s$ is the rotation matrix corresponding to side s and $\mathbf{T}_s^{-1}$ is its inverse, $\mathbf{F}_{(i,s)}$ is the numerical flux for face s in the direction normal to it, and is obtained by solving the Riemann problem

$$\left.\begin{array}{l} \partial_\tau \mathbf{Q} + \partial_d \mathbf{F}(\mathbf{Q}) = \mathbf{0} \ , \\ \\ \mathbf{Q}(d,0) = \left\{ \begin{array}{lll} \mathbf{Q}_i^0 & \equiv \mathbf{T}_s(\mathbf{Q}_i^n) & \text{if} \quad d < 0 \ , \\ \mathbf{Q}_{i+1}^0 & \equiv \mathbf{T}_s(\mathbf{Q}_s^n) & \text{if} \quad d > 0 \ . \end{array} \right. \end{array}\right\} \tag{4}$$

Here d is distance normal to face s; $\tau = t - t^n$ is local time; $\mathbf{Q}_s^n$ is the integral average of the conserved variable vector in the control volume adjacent to V_i having s as a common face; T_s aligns the original initial data in the direction normal to the interface s, prior to solving the Riemann problem. The inverse matrix T_s^{-1} restores back the flux information to the Cartesian frame.

From this point on, the discussion on the numerical flux in an arbitrary direction s can be reduced to that of the *augmented* one-dimensional problem in the x-direction, without loosing generality.

2.2 The Riemann Problem and the Godunov Flux

The one-dimensional equations and the corresponding one-dimensional finite volume scheme are:

$$\left.\begin{array}{l} \partial_t \mathbf{Q} + \partial_x \mathbf{F}(\mathbf{Q}) = \mathbf{0} \ , \\ \\ \mathbf{Q}_i^{n+1} = \mathbf{Q}_i^{n+1} - \frac{\Delta t}{\Delta x} [\mathbf{F}_{i+\frac{1}{2}} - \mathbf{F}_{i-\frac{1}{2}}] \ , \end{array}\right\} \tag{5}$$

where $\mathbf{F}_{i+\frac{1}{2}}$ is the numerical flux. Godunov's method [9] defines the intercell numerical flux $\mathbf{F}_{i+\frac{1}{2}}$ in terms of the solution of the corresponding Riemann problem

$$\left.\begin{array}{l} \partial_t \mathbf{Q} + \partial_x \mathbf{F}(\mathbf{Q}) = \mathbf{0} \ , \\ \\ \mathbf{Q}(x,0) = \left\{ \begin{array}{lll} \mathbf{Q}_i^n \ , & \text{if} & x < 0 \ , \\ \mathbf{Q}_{i+1}^n \ , & \text{if} & x > 0 \ . \end{array} \right. \end{array}\right\} \tag{6}$$

Fig. 1 shows the structure of the solution of the Riemann problem in the x-t plane for an $m \times m$ non-linear system. The so-called *Riemann fan* consists of $m+1$ constant states separated by m wave families, each one associated with a real eigenvalue $\lambda^{(k)}$. The similarity solution of (6) depends of the ratio x/t and is denoted by $\mathbf{Q}_{i+\frac{1}{2}}(x/t)$. The Godunov intercell numerical flux is found by first evaluating $\mathbf{Q}_{i+\frac{1}{2}}(x/t)$ at $x/t = 0$, that is along the t-axis in Fig. 1, and then evaluating the physical flux vector $\mathbf{F}(\mathbf{Q})$ in (5) at $\mathbf{Q}_{i+\frac{1}{2}}(0)$, namely

$$\mathbf{F}_{i+\frac{1}{2}}^{God} = \mathbf{F}(\mathbf{Q}_{i+\frac{1}{2}}(0)) \ . \tag{7}$$

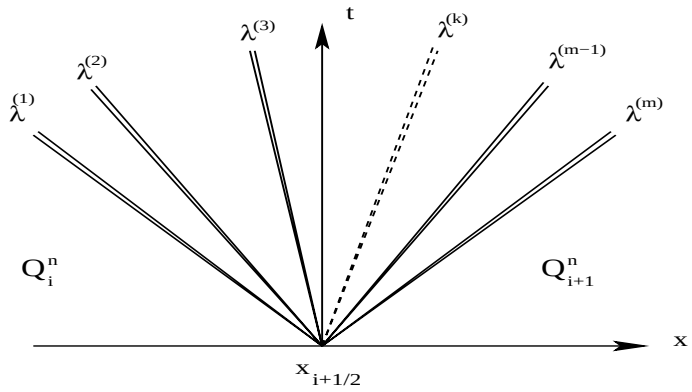

Figure 1: Structure of the solution of the Riemann problem for an $m \times m$ hyperbolic system.

The exact solution will generally involve at least one iterative procedure and thus in practice, whenever possible, one uses approximate Riemann solvers. For a review on Riemann solvers see, for example, [29].

2.3 Centred Fluxes

We briefly review intercell numerical fluxes of the centred type to be used directly into the conservative formula in (5). Unlike upwind methods, centred fluxes do not make use of the solution of the Riemann problem and they can generally be computed explicitly as functions of the initial data, namely

$$\mathbf{F}_{i+\frac{1}{2}} = \mathbf{F}_{i+\frac{1}{2}}(\mathbf{Q}_i^n, \mathbf{Q}_{i+1}^n) \; . \tag{8}$$

One may interpret centred fluxes as resulting from a *low-level approximation* to the solution of the Riemann problem (6), in which the Riemann fan *is not opened*. See Fig. 1.

Two classical centred fluxes are the Lax-Friedrichs flux

$$\mathbf{F}_{i+\frac{1}{2}}^{LF} = \mathbf{F}_{i+\frac{1}{2}}^{LF}(\mathbf{Q}_i^n, \mathbf{Q}_{i+1}^n) = \frac{1}{2}[\mathbf{F}(\mathbf{Q}_i^n) + \mathbf{F}(\mathbf{Q}_{i+1}^n)] - \frac{1}{2}\frac{\Delta x}{\Delta t}[\mathbf{Q}_{i+1}^n - \mathbf{Q}_i^n] \tag{9}$$

and the two-step Lax-Wendroff flux

$$\left.\begin{array}{l} \mathbf{F}_{i+\frac{1}{2}}^{LW} = \mathbf{F}_{i+\frac{1}{2}}^{LW}(\mathbf{Q}_i^n, \mathbf{Q}_{i+1}^n) = \mathbf{F}(\mathbf{Q}_{i+\frac{1}{2}}^{n+\frac{1}{2}}) \; , \\ \mathbf{Q}_{i+\frac{1}{2}}^{n+\frac{1}{2}} = \frac{1}{2}[\mathbf{Q}_i^n + \mathbf{Q}_{i+1}^n] - \frac{1}{2}\frac{\Delta t}{\Delta x}[\mathbf{F}(\mathbf{Q}_{i+1}^n) - \mathbf{F}(\mathbf{Q}_i^n)] \; . \end{array}\right\} \tag{10}$$

Another, more recent, centred flux is the FORCE flux, which was derived [28] from a deterministic interpretation of the staggered-grid version of Glimm's method [7] and results in a non-staggered one-step conservative scheme of the form (5) with intercell numerical flux given by

$$\mathbf{F}_{i+\frac{1}{2}}^{\text{force}} = \mathbf{F}_{i+\frac{1}{2}}^{\text{force}}(\mathbf{Q}_i^n, \mathbf{Q}_{i+1}^n) = \frac{1}{4}\left[\mathbf{F}(\mathbf{Q}_i^n) + 2\mathbf{F}(\mathbf{Q}_{i+\frac{1}{2}}^{n+\frac{1}{2}}) + \mathbf{F}(\mathbf{Q}_{i+1}^n) - \frac{\Delta x}{\Delta t}\left(\mathbf{Q}_{i+1}^n - \mathbf{Q}_i^n\right)\right] \; , \tag{11}$$

with $\mathbf{Q}_{i+\frac{1}{2}}^{n+\frac{1}{2}}$ as in (10). For further details on the FORCE flux see also [29], [30], [2].

A surprising outcome is that the intercell flux (11) is in fact the arithmetic mean of the Lax-Wendroff flux $\mathbf{F}_{i+\frac{1}{2}}^{LW}$ and the Lax-Friedrichs flux $\mathbf{F}_{i+\frac{1}{2}}^{LF}$. A whole class of centred fluxes can

be constructed by considering convex averages of the form

$$\mathbf{F}^{\omega}_{i+\frac{1}{2}} = \omega \mathbf{F}^{LF}_{i+\frac{1}{2}} + (1-\omega)\mathbf{F}^{LW}_{i+\frac{1}{2}} \, , \tag{12}$$

with ω a real number in $[0,1]$. Then the FORCE flux is a particular member of this class with $\omega = \frac{1}{2}$. As we shall see FORCE is in fact the optimal scheme in this class.

Insight on the resulting centred schemes is gained by considering the model hyperbolic equation $\partial_t q + \lambda \partial_x q = 0$, where λ is a given constant wave speed. Fig. 2 shows a plot containing the family of three-point schemes that can be written as (12), where the bottom boundary (maximum numerical dissipation) corresponds to the Lax-Friedrichs scheme (LF) and the top boundary (minimum numerical dissipation) corresponds to the Lax-Wendroff scheme (LW). The whole region is subdivided into a bottom region of monotone schemes, for $\omega \leq \omega_g \equiv \frac{1}{1+c}$, and an upper region of non-monotone schemes, for which $\omega > \omega_g$. Here c is the Courant number. The line $\omega = \frac{1}{1+c}$ corresponds precisely to the Godunov first-order upwind scheme, which is the first-order scheme with the smallest numerical dissipation and monotone, the best scheme. Also shown in Fig. 2 is the weight for the Godunov first-order centred method [10], which is linearly stable for $0 \leq c \leq \frac{1}{2}\sqrt{2}$, but is not monotone in the range $0 \leq c \leq \frac{1}{2}$. If we were to select an average (12) with constant weight ω (independent of wave propagation information), then the scheme with the smallest numerical dissipation and monotone would be the $FORCE$ scheme. In this sense, the FORCE flux is the optimal flux that does not make explicit use of wave propagation information. Moreover, in [2] it is shown that the conservative scheme in (5) with the FORCE flux (11) is convergent, for a 2×2 non-linear system of conservation laws. The multi-stage flux schemes of this paper are based on the FORCE flux as predictor and corrector.

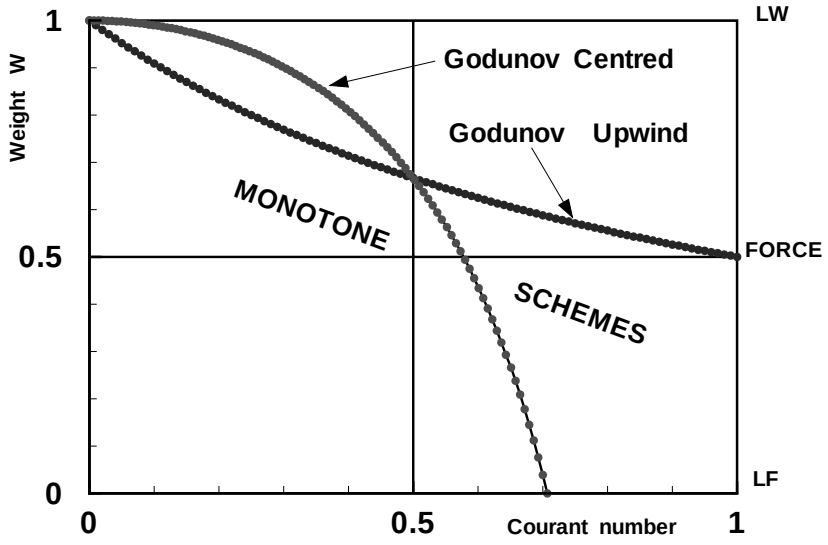

Figure 2: Family of fluxes for three-point schemes as convex average of the Lax-Friedrichs (LF) and Lax-Wendroff (LW) fluxes.

3 The Multi-stage MUSTA Flux

Given two adjacent data states $\mathbf{Q}^n_i$ and $\mathbf{Q}^n_{i+1}$, a corresponding intercell numerical flux $\mathbf{F}_{i+\frac{1}{2}}$ at the interface $x_{i+\frac{1}{2}}$ is sought. In this section we present a multi-stage procedure to compute the

numerical flux in a way that the Riemann fan is *opened*, without having to solve the Riemann problem in the conventional way. See Fig. 1.

3.1 The Basic Scheme

In the MUSTA flux approach we first evolve in time the data states, for a number of stages, utilizing a predictor flux function $\mathbf{F}^{(p)}$. In this manner, starting with $\mathbf{Q}_i^{(0)} = \mathbf{Q}_i^n$ and $\mathbf{Q}_{i+1}^{(0)} = \mathbf{Q}_{i+1}^n$, after k stages we have the evolved data $\mathbf{Q}_i^{(k)}$ and $\mathbf{Q}_{i+1}^{(k)}$. The sought numerical flux is computed by using a *corrector* flux function $\mathbf{F}^{(c)}(V, W)$, in which the arguments are the evolved states.

Consider Fig. 3 in the $s - \tau$ plane. Assume that at stage $k-1$ the two initial data states $\mathbf{Q}_i^{(k-1)}$ and $\mathbf{Q}_{i+1}^{(k-1)}$ adjacent to the interface $i + \frac{1}{2}$ are known. We need to determine the states at the next stage k. Note that Fig. 3 also depicts two additional states to the left and right. Integration of the differential equations in (5) in space s and time τ on the control volumes

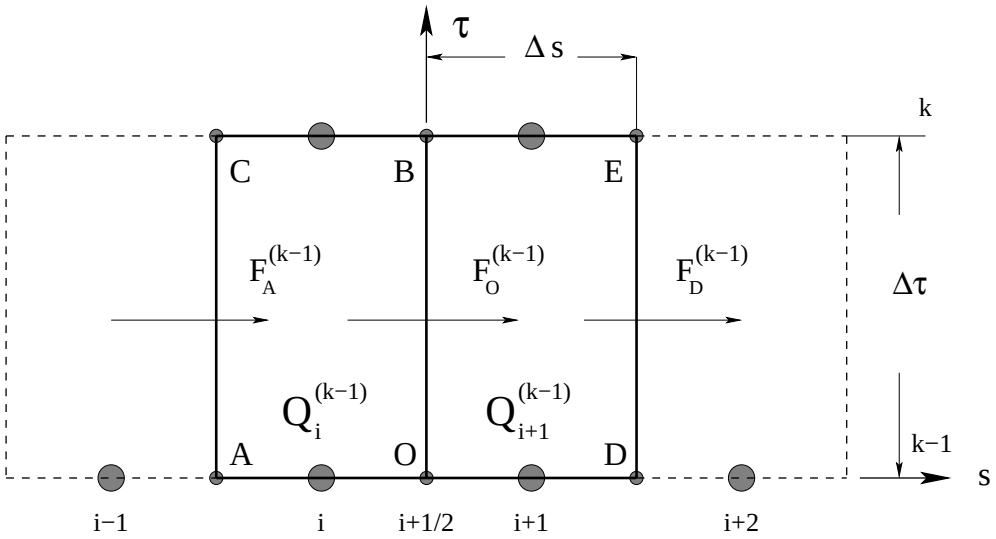

Figure 3: Illustration of the multi-stage procedure.

$OBCD$ and $ODEB$ yields, respectively

$$\left.\begin{aligned} \mathbf{Q}_i^{(k)} &= \mathbf{Q}_i^{(k-1)} - \tfrac{\Delta\tau}{\Delta s}[\mathbf{F}_{OB}^{(k-1)} - \mathbf{F}_{AC}^{(k-1)}]\,, \\ \mathbf{Q}_{i+1}^{(k)} &= \mathbf{Q}_{i+1}^{(k-1)} - \tfrac{\Delta\tau}{\Delta s}[\mathbf{F}_{DE}^{(k-1)} - \mathbf{F}_{OB}^{(k-1)}]\,, \end{aligned}\right\} \tag{13}$$

with the usual definitions for space and time integral averages. Given that the Riemann data extends to $-\infty$ and ∞, at each stage, we set

$$\mathbf{Q}_{i-1}^{(k-1)} = \mathbf{Q}_i^{(k-1)}; \quad \mathbf{Q}_{i+2}^{(k-1)} = \mathbf{Q}_{i+1}^{(k-1)}\,, \tag{14}$$

so that the outer fluxes at interfaces AC and DE can be computed thus

$$\mathbf{F}_{AC}^{(k-1)} = \mathbf{F}(\mathbf{Q}_i^{(k-1)}); \quad \mathbf{F}_{DE}^{(k-1)} = \mathbf{F}(\mathbf{Q}_{i+1}^{(k-1)}) \tag{15}$$

and therefore formulae (13) become

$$\left.\begin{aligned} \mathbf{Q}_i^{(k)} &= \mathbf{Q}_i^{(k-1)} - \tfrac{\Delta\tau}{\Delta s}[\mathbf{F}_{OB}^{(k-1)} - \mathbf{F}(\mathbf{Q}_i^{(k-1)})];, \\ \mathbf{Q}_{i+1}^{(k)} &= \mathbf{Q}_{i+1}^{(k-1)} - \tfrac{\Delta\tau}{\Delta s}[\mathbf{F}(\mathbf{Q}_{i+1}^{(k-1)}) - \mathbf{F}_{OB}^{(k-1)}];, \end{aligned}\right\} \tag{16}$$

where

$$\mathbf{F}_{OB}^{(k-1)} = \mathbf{F}^{(p)}(\mathbf{Q}_i^{(k-1)}, \mathbf{Q}_{i+1}^{(k-1)}) \tag{17}$$

is a *predictor* flux, yet to be specified. The final MUSTA flux is then

$$\mathbf{F}_{i+\frac{1}{2}}^{MUSTA} = \mathbf{F}^{(c)}(\mathbf{Q}_i^{(k)}, \mathbf{Q}_{i+1}^{(k)}) \ , \tag{18}$$

where $\mathbf{F}^{(c)}(\mathbf{V}, \mathbf{W})$ is a corrector numerical flux.

In this paper we propose **MUSTA**-type schemes based on applying the $FORCE$ flux [28] for both the predictor and the corrector steps, namely

$$\mathbf{F}^{(p)}(U, V) = \mathbf{F}^{(c)}(U, V) = \mathbf{F}_{i+\frac{1}{2}}^{FORCE}(U, V) \ . \tag{19}$$

Also, we set $\Delta\tau = \Delta t$ and $\Delta s = \Delta x$, where Δt and Δx are related by the CFL stability condition that comes from the numerical scheme being applied.

An algorithm of the MUSTA scheme works as follows. The multi-staging is started by setting $l = 0$, $\mathbf{Q}_i^{(0)} = \mathbf{Q}_i^n$ and $\mathbf{Q}_{i+1}^{(0)} = \mathbf{Q}_{i+1}^n$. We then do the following:

$$\left.\begin{aligned} &\textbf{Step 1: Flux evaluation} \\ &\left.\begin{aligned} &\mathbf{F}_i^{(l)} = \mathbf{F}(\mathbf{Q}_i^{(l)}) \ , \ \ \mathbf{F}_{i+1}^{(l)} = \mathbf{F}(\mathbf{Q}_{i+1}^{(l)}) \ , \\ &\mathbf{Q}_{i+\frac{1}{2}}^{(l)} = \tfrac{1}{2}[\mathbf{Q}_i^{(l)} + \mathbf{Q}_{i+1}^{(l)}] - \tfrac{1}{2}\tfrac{\Delta t}{\Delta x}[\mathbf{F}_{i+1}^{(l)} - \mathbf{F}_i^{(l)}] \ , \ \ \mathbf{F}_M^{(l)} = \mathbf{F}(\mathbf{Q}_{i+\frac{1}{2}}^{(l)}) \ , \\ &\mathbf{F}_{i+\frac{1}{2}}^{(l)} = \tfrac{1}{4}\left[\mathbf{F}_i^{(l)} + 2\mathbf{F}_M^{(l)} + \mathbf{F}_{i+1}^{(l)} - \tfrac{\Delta x}{\Delta t}\left(\mathbf{Q}_{i+1}^{(l)} - \mathbf{Q}_i^{(l)}\right)\right] \ . \end{aligned}\right\} \\ &\text{If the prescribed number of stages K has been reached, STOP.} \\ &\text{Otherwise} \\ &\textbf{Step 2: Opening of Riemann fan} \\ &\mathbf{Q}_i^{(l+1)} = \mathbf{Q}_i^{(l)} - \tfrac{\Delta t}{\Delta x}[\mathbf{F}_{i+\frac{1}{2}}^{(l)} - \mathbf{F}_i^{(l)}] \ , \ \ \mathbf{Q}_{i+1}^{(l+1)} = \mathbf{Q}_{i+1}^{(l)} - \tfrac{\Delta t}{\Delta x}[\mathbf{F}_{i+1}^{(l)} - \mathbf{F}_{i+\frac{1}{2}}^{(l)}] \ . \\ &\textbf{Step 3: Goto step 1} \end{aligned}\right\} \tag{20}$$

A few remarks are in order. First a question of notation. A K-stage MUSTA flux will be denoted by $MUSTA_K$. Note that the trivial case, $MUSTA_0$, simply corresponds to the predicter/corrector flux (the FORCE flux here) applied to the original data. Also, it is easy to verify that the numerical flux resulting from the corrector step is *consistent* if the fluxes employed in both the predictor and corrector steps are consistent. That is, for $\mathbf{Q}_i^n = \mathbf{Q}_{i+1}^n = \bar{\mathbf{Q}}$ we have

$$\mathbf{F}_{i+\frac{1}{2}} = \mathbf{F}_{i+\frac{1}{2}}(\mathbf{Q}_i^n, \mathbf{Q}_{i+1}^n) = \mathbf{F}_{i+\frac{1}{2}}(\bar{\mathbf{Q}}, \bar{\mathbf{Q}}) = \mathbf{F}(\bar{\mathbf{Q}}) \ . \tag{21}$$

As the $MUSTA_0$ flux corresponds to the FORCE scheme, we remark that in [2] this scheme is shown to be convergent when applied to a 2×2 non-linear hyperbolic system. In [26] we carried out preliminary analysis of the properties of the $MUSTA_1$ scheme, in terms of the model linear advection equation. Further analysis for the $MUSTA_K$ schemes is the subject of current research.

Regarding the question of efficiency. For a K-stage $MUSTA_K$ scheme the number of elementary arithmetic operations needed for the evaluation of the intercell numerical flux is roughly $K(3$ flux evaluations $+11m + 8) - 4m - 2$, where m is the number of equations of the system. There are no fractional powers involved, unless they are present at the level of the equation of state, for example, via the flux evaluations in Step 1 in (20). For the one-dimensional Euler equations ($m = 3$), a 1-stage scheme $MUSTA_1$ requires 68 operations and three flux evaluations. This is comparable to typical existing approximate Riemann solvers, such as Roe's solver [20] or the HLLC solver [32], for example, but much more efficient than the approximate Riemann solver of Osher and Solomon [19]. As will be illustrated through numerical experiments in section 4, the $MUSTA_K$ flux achieves the accuracy of the best Riemann solvers available, and it does so preserving simplicity and generality.

3.2 Non-Conservative Variant of MUSTA

We note here that the MUSTA predictor as well as corrector steps are by no means restricted to conservative-type schemes. The states $\mathbf{Q}_i^{(k)}, \mathbf{Q}_{i+1}^{(k)}$ may be found by other procedures. For example, we may write the governing equations in (5) in non-conservative form

$$\partial_t \mathbf{W} + \mathbf{A}\left(\mathbf{W}\right) \partial_x \mathbf{W} = \mathbf{0} \ , \tag{22}$$

where $\mathbf{W}$ is a vector of suitably chosen variables; they could also be the conservative variables. A corresponding MUSTA predictor step is

$$\left.\begin{array}{l} \mathbf{W}_i^{(l+1)} = \mathbf{W}_i^{(l)} - \frac{\Delta t}{\Delta x} \mathbf{A}_i^{(l)} [\mathbf{W}_{i+\frac{1}{2}}^{(l)} - \mathbf{W}_i^{(l)})] \ , \\ \mathbf{W}_{i+1}^{(l+1)} = \mathbf{W}_{i+1}^{(l)} - \frac{\Delta t}{\Delta x} \mathbf{A}_{i+1}^{(l)} [\mathbf{W}_{i+1}^{(l)} - \mathbf{W}_{i+\frac{1}{2}}^{(l)})] \ . \end{array}\right\} \tag{23}$$

Here $\mathbf{W}_{i+\frac{1}{2}}^{(l)}$ is a suitable *intermediate* vector; see Toro and Siviglia [34] for possible choices for intermediate vectors arising from non-conservative centred schemes. The coefficient matrices are

$$\mathbf{A}_i^{(l)} = \mathbf{A}(\mathbf{W}_i^{(l)}) \ , \quad \mathbf{A}_{i+1}^{(l)} = \mathbf{A}(\mathbf{W}_{i+1}^{(l)}) \ . \tag{24}$$

This approach for evaluating the evolved interface states also has potential for the construction of numerical schemes for non-conservative hyperbolic systems.

3.3 Extensions: Higher Accuracy and Multiple Space Dimensions

The MUSTA first-order schemes just presented may be extended to second or higher-order of accuracy following a variety of standard ways. Here we present a possible second-order TVD scheme following the MUSCL-Hancock approach [38], whereby one considers reconstructed data via piece-wise linear polynomials, so that in each cell i we have two boundary extrapolated values

$$\mathbf{Q}_i^L = \mathbf{Q}_i^n - \frac{1}{2}\Delta_i \ , \quad \mathbf{Q}_i^R = \mathbf{Q}_i^n + \frac{1}{2}\Delta_i \ , \tag{25}$$

where Δ_i is a TVD *limited* slope. These boundary extrapolated values are then evolved in time by half a time step as follows:

$$\hat{\mathbf{Q}}_i^L = \mathbf{Q}_i^L - \frac{1}{2}\frac{\Delta t}{\Delta x}[\mathbf{F}(\mathbf{Q}_i^R) - \mathbf{F}(\mathbf{Q}_i^L)] \ , \ \ \hat{\mathbf{Q}}_i^R = \mathbf{Q}_i^R - \frac{1}{2}\frac{\Delta t}{\Delta x}[\mathbf{F}(\mathbf{Q}_i^R) - \mathbf{F}(\mathbf{Q}_i^L)] \ . \tag{26}$$

Finally, the MUSTA flux is computed by applying algorithm (20) with initial conditions

$$\mathbf{Q}_i^{(0)} = \hat{\mathbf{Q}}_i^R \ \text{ and } \ \mathbf{Q}_{i+1}^{(0)} = \hat{\mathbf{Q}}_{i+1}^L \ .$$

For details on the MUSCL-Hancock scheme see [29].

The extension of this TVD scheme to multi-dimensional problems can be carried in at least two ways. The simplest method is dimensional splitting. Another possibility is a simultaneous updating, unsplit finite volume approach, as given by (3). See [29], Chapt. 16 for details on these two approaches. We note, however, that the simultaneous updating unsplit finite volume approach (explicit) is conditionally stable for upwind intercell fluxes but not for centred fluxes such as the Lax-Friedrichs flux and the FORCE flux. See [30].

We have implemented the $MUSTA_K$ flux for both split and unsplit schemes in two and three space dimensions, using TVD methods and WENO methods. In this paper we show results for the two-dimensional Euler equations for non-Cartesian geometries using the second-order Strang splitting [23].

4 Numerical Results

To illustrate the performance of the methods proposed in this paper we solve the time-dependent Euler equations in one space dimension and in two space dimensions on non-Cartesian geometries. We use the ideal gas equation of state with constant gamma $\gamma = 1.4$. We compare the results with exact solutions and with reference solutions. Each of the test problems chosen has a particular purpose in mind.

4.1 Test 1: a shock tube problem with sonic flow

The main purpose of this test problem is to assess the performance of the methods in the presence of *sonic flow*. We solve the one-dimensional Euler equations in the domain $[0, 1]$, subdivided into a left section $[0, 0.3)$ and a right section $[0.3, 1]$. The initial conditions assign data for density, velocity and pressure $\rho_L = 1.0$, $u_L = 3/4$, $p_L = 1.0$ in the left section and $\rho_R = 1/8$, $u_R = 0.0$, $p_R = 0.1$ in the right section. The solution includes a right shock, a right contact discontinuity and a left *transonic*, or *sonic* rarefaction wave. We remark that this is not the original Sod test problem but a modification of it, in order to produce a transonic rarefaction as part of the solution. The *sonic point* is known to cause difficulties to most numerical methods, particularly to those based on linearized Riemann solvers, for which an explicit *entropy fix* must be built into the scheme to avoid the computation of *rarefaction shocks*. Here the computations are carried out using $M = 100$ cells and a CFL number of 0.9. We apply transmissive boundary condition at both ends.

Results for density are shown in Figs. 5 and 6 for the $MUSTA_3$ scheme, where the exact solution is shown by a full line. Regarding the results of the $MUSTA_3$ scheme, shown in Fig. 4, two points are noted. First, the numerical solution, shown by symbols, is seen to be free from spurious oscillations in the vicinity of discontinuities. Secondly, the performance of the scheme

at the sonic point inside the transonic rarefaction, $x \approx 0.3$, is very satisfactory; the $MUSTA_3$ solution within the rarefaction is very smooth, as it should be. Fig. 6 shows, in addition to the exact solution given by the full line, a comparison between the Godunov first-order upwind method used in conjunction with the exact Riemann solver (dashed line) and the $MUSTA_3$ scheme (full smooth line). It is seen that the two schemes are indistinguishable at the shock wave. Elsewhere, the $MUSTA_3$ solution is more accurate, as is clearly seen in the vicinity of the the contact wave and the sonic point. The $MUSTA_3$ flux is distinctly better for the sonic point and this is achieved automatically by the MUSTA scheme, no ad-hoc entropy fixes are required.

Fig. 7 shows MUSTA (firt-order mode) numerical results for density (shown in symbols) and the exact solution (line) for a sequence of four meshes of 100, 200, 400 and 800 cells. The expected behaviour of the numerical solution under mesh refinement is observed. Convergence for the shock wave is fast, it is slower for the rarefaction wave and much slower for the contact discontinuity. This behaviour is typical of other numerical methods as applied to this kind of test problems. The behaviour of second-order TVD extension of MUSTA under mesh refinement is illustrated in Fig. 8. These results are to be compared with those of Fig. 7.

4.2 Test 2: A Blast Wave Problem

The purpose of this test problem is to assess the robustness and accuracy of the $MUSTA_K$ schemes for a problem involving very strong shock waves and multiple wave interaction. This problem does not have an exact solution. As the reference solution we take that obtained by the Godunov first order upwind scheme used in conjunction with the exact Riemann solver. Recall that this is the scheme with the smallest truncation error, amongst all first-order monotone schemes. It is the scheme we are trying to emulate. We solve the blast wave problem proposed by Woodward and Colella [39]. The domain consists of a tube of unit length with three sections, a left section $[0.0, 0.1)$, a middle section $[0.1, 0.9)$ and a right section $[0.9, 1.0]$. The initial values for density and particle velocity throughout the domain are $\rho = 1.0$, $u = 0.0$, whereas the initial pressure takes on the following three values $p_L = 1000.0$ in the left section, $p_M = 0.01$ in the middle section and $p_R = 100.0$ in the right section. Reflective boundary conditions are imposed at both ends. The solution of this problem is very complex and involves multiple wave interaction, as time evolves. For a detailed discussion on the solution see [39]. For all methods we used a CFL number of 0.9 and a mesh of 3000 cells.

Figs. 9 and 10 show numerical results for density at the output time $t = 0.038$ in the interesting section $[\frac{1}{2}, 0.9]$. The first feature of the solution, from the left is a contact discontinuity; the second feature from the left is a shock wave. The first feature from the right is also a shock wave and the second feature from the right is a contact discontinuity. Fig. 9 shows a comparison between two first-order monotone methods, namely the Lax-Friedrichs scheme (symbols) and the Godunov first-order upwind scheme with the exact Riemann solver. The discrepancy is not surprising, the Lax-Friedrichs scheme is the most diffusive of all stable, three-point monotone first-order schemes. Fig. 10 shows the result from the 3-stage $MUSTA_3$ scheme, which is virtually indistinguishable from that of the Godunov scheme with the exact Riemann solver. As a matter of fact, the $MUSTA_3$ solution is slightly more accurate than the Godunov solution; this was also observed to be the case for Test 1. We find that the 2-stage $MUSTA_2$ is sufficiently accurate and is probably the scheme to be used for practical computations.

4.3 Test 3: Shock Reflection in Two Space Dimensions

This test consists of a shock reflection problem in a two-dimensional non-Cartesian domain as depicted by the left-hand side sketch of Fig. 4. This is a double-wedge situation in which a plane shock wave travels from left to right, reflects from the wedges placed at an angle of 25 degrees to the initial shock direction, producing a symmetric Mach reflection pattern. The right-hand side picture of Fig. 4 shows the experimental result for a single wedge, that is, the lower half of the domain shown on the left-hand side. Clearly seen in the experiment are the incident shock, the reflected shock, the Mach stem and the slip surface, all meeting at the triple point. The experiment corresponds to an initial shock wave of shock Mach number 1.7. Numerical results are given in Figs. 11 to 14, in which contours are shown for 80 equally spaced levels.

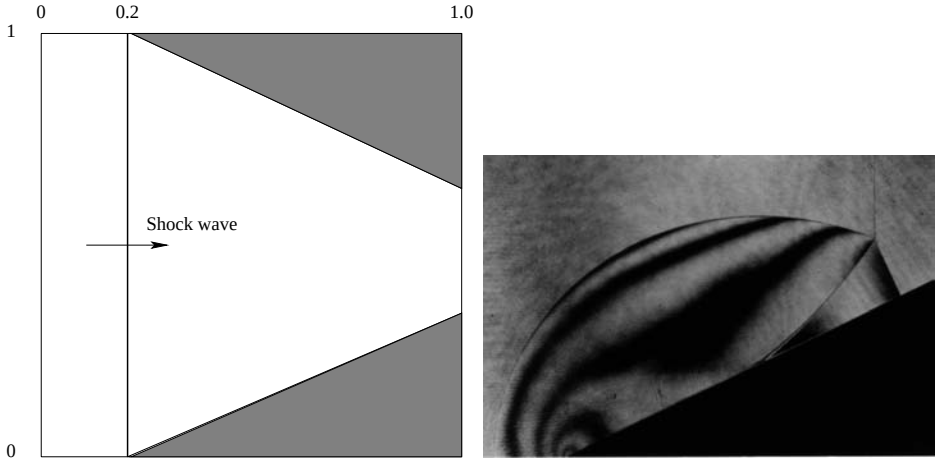

Figure 4: Test 3. Shock reflection problem. Left-hanside sketch shows computational domain and position of initial shock wave. Right-hand side picture shows the experimental result for the lower half of the domain (Courtesy Prof. K Takayama, Japan).

Fig. 11 shows computed results at the output time $t = 1.0\ ms$ using a mesh of $M3 = 1000 \times 1000$ cells and a CFL number of 0.9. The qualitative agreement between the experimental result of Fig. 4 (right-hand side) and the numerical result of Fig. 11 is very satisfactory. All features seen in the experiment are reproduced in the numerical solution. The numerical results have also preserved the expected symmetry of the problem. Note also that our results do not escape the typical, so-called, *start-up error*, which is clearly seen in the density plots. There are standard ways of eliminating this error but we do not believe this is worth implementing.

The numerical resolution of all discontinuities is very satisfactory; discontinuities are sharp and free from spurious oscillations. For modern numerical methods the resolution of shocks is usually straightforward, but not so the resolution of linearly degenerate fields, for which one of the problems to be encountered is excessive numerical diffusion. Our results also show a good resolution of the slip surfaces emanating from the triple points. To assess the convergence properties of the scheme we computed solutions of the same problem using two more, coarser, meshes. The results are shown in Figs. 12 and 13. Compare the succession of results from Figs. 12, 13 and 11, in which the mesh refinement factor is 2.

Finally, Fig. 14 shows the numerical solution at time $t = 1.1\ ms$ using the mesh $M3 = 1000 \times 1000$ cells and a CFL number of 0.9. Note that the two reflected shock waves have interacted producing two new, stronger reflected shocks waves. This computation is included to demonstrate the ability of the scheme to handle strong wave interaction in multiple space

dimensions.

5 Concluding remarks

We have presented a multi-stage (MUSTA) approach to obtain an upwind numerical flux for use in finite volume and discontinuous Galerkin finite element methods when solving general hyperbolic systems. The implementation presented here relies on using the FORCE centred flux at each stage. It is demonstrated that the resulting MUSTA flux, in its first-order mode, is capable of attaining the accuracy of the reference first-order scheme, namely the Godunov method used in conjunction with the exact Riemann solver. The MUSTA flux is applicable to any system of conservation laws, regardless of their complexity. The schemes can be applied to multi-dimensional problems in the setting of finite volume and discontinuous Galerkin finite element methods. High-order extensions are also possible following any of the current approaches, such as TVD methods, ENO/WENO methods, ADER methods and discontinuous Galerkin methods. In this paper we have shown extensions of the TVD type for the two-dimensional Euler equations on non-Cartesian domains. Work in progress includes the implementation of the MUSTA flux in the WENO schemes for three dimensional systems and the solution of compressible multi-phase flow problems.

Acknowledgments. This work was carried out while the author was an EPSRC senior visiting fellow (Grant GR N09276) at the Isaac Newton Institute for Mathematical Sciences, University of Cambridge, UK, as joint organizer (with P. G. LeFloch and C. M. Dafermos) of the research programme *Non-linear Hyperbolic Waves in Phase Dynamics and Astrophysics*, Cambridge, January to July 2003. The support provided is gratefully acknowledged.

I am also indebted to Vladimir Titarev (University of Trento, Italy) and Prof. Sam Falle (University of Leeds, UK) for useful discussions on the MUSTA flux and related topics.

References

[1] M. Ben-Artzi and J. Falcovitz. *Generalized Riemann Problems in Computational Fluid Dynamics*. Cambridge University Press, 2003.

[2] G. Q. Chen and E. F. Toro. Centred schemes for non-linear hyperbolic equations. Technical Report to appear, Isaac Newton Institute for Mathematical Sciences, University of Cambridge, UK, 2003.

[3] B. Cockburn and C. W. Shu. TVB Runge–Kutta Local Projection Discontinuous Galerkin Method for Conservation Laws II: General Framework. *Math. Comput.*, 52(–):411–, 1989.

[4] P. Colella. A Direct Eulerian MUSCL Scheme for Gas Dynamics. *SIAM J. Sci. Stat. Comput.*, 6:104–117, 1985.

[5] R. Courant, E. Isaacson, and M. Rees. On the Solution of Nonlinear Hyperbolic Differential Equations by Finite Differences. *Comm. Pure. Appl. Math.*, 5:243–255, 1952.

[6] Kolgan N. E. Application of the Principle of Minimum Derivatives to the Construction of Difference Schemes for Computing Discontinuous Solutions of Gas dynamics (in Russian). *Uch. Zap. TsaGI, Russia*, 6, 1972.

[7] J. Glimm. Solution in the Large for Nonlinear Hyperbolic Systems of Equations. *Comm. Pure. Appl. Math.*, 18:697–715, 1965.

[8] E. Godlewski and P. A. Raviart. *Numerical Approximation of Hyperbolic Systems of Conservation Laws*. Springer, 1996.

[9] S. K. Godunov. Finite Difference Methods for the Computation of Discontinuous Solutions of the Equations of Fluid Dynamics. *Mat. Sb.*, 47:271–306, 1959.

[10] S. K. Godunov, A. V. Zabrodin, and G. P. Prokopov. –. *J. Comp. Math. Phys. USSR 1 (1962)*, pages 1187–, 1962.

[11] A. Harten. High Resolution Schemes for Hyperbolic Conservation Laws. *J. Comput. Phys.*, 49:357–393, 1983.

[12] A. Harten, B. Engquist, S. Osher, and S. R. Chakravarthy. Uniformly High Order Accuracy Essentially Non–oscillatory Schemes III. *J. Comput. Phys.*, 71:231–303, 1987.

[13] A. Harten and S. Osher. Uniformly High–Order Accurate Nonoscillatory Schemes I. *SIAM J. Numer. Anal.*, 24(2):279–309, 1987.

[14] C. B. Laney. *Computational Gasdynamics*. Cambridge University Press, 1998.

[15] P. D. Lax and B. Wendroff. Systems of Conservation Laws. *Comm. Pure Appl. Math.*, 13:217–237, 1960.

[16] R. J. LeVeque. *Numerical Methods for Conservation Laws*. Birkhäuser Verlag, 1992.

[17] D. Levy, G. Puppo, and G. Russo. Central WENO Schemes for Hyperbolic Systems of Conservation Laws. *Mathematical Modelling and Numerical Analysis*, 33:547–571, 1999.

[18] H. Nessyahu and E. Tadmor. Non–oscillatory Central Differencing for Hyperbolic Conservation Laws. *J. Comput. Phys.*, 87:408–463, 1990.

[19] S. Osher and F. Solomon. Upwind Difference Schemes for Hyperbolic Conservation Laws. *Math. Comp.*, 38,158:339–374, 1982.

[20] P. L. Roe. Approximate Riemann Solvers, Parameter Vectors, and Difference Schemes. *J. Comput. Phys.*, 43:357–372, 1981.

[21] T. Schwartzkopff, Munz C.D, and E. F. Toro. ADER: High-Order Approach for Linear Hyperbolic Systems in 2D. *J. Scientific Computing*, 17:231–240, 2002.

[22] C. W. Shu. Essentially Non–oscillatory and Weighted Non–oscillatory Schemes for Hyperbolic Conservation Laws. Technical Report ICASE Report No. 97–65, NASA, 1997.

[23] G. Strang. On the Construction and Comparison of Difference Schemes. *SIAM J. Numer. Anal.*, 5(3):506–517, 1968.

[24] Y. Takakura and E. F. Toro. Arbitrarily Accurate Non-Oscillatory Schemes for a Non-Linear Conservation Law. *J. Computational Fluid Dynamics*, 11(1):7–18, 2002.

[25] V. A. Titarev and E. F. Toro. ADER: Arbitrary High Order Godunov Approach. *J. Scientific Computing*, 17:609–618, 2002.

[26] E. F. Toro. Multi-Stage Predictor-Corrector Fluxes for Hyperbolic Equations. Technical Report NI03037-NPA, Isaac Newton Institute for Mathematical Sciences, University of Cambridge, UK, 17th June, 2003.

[27] E. F. Toro. A Weighted Average Flux Method for Hyperbolic Conservation Laws. *Proc. Roy. Soc. London*, A423:401–418, 1989.

[28] E. F. Toro. On Glimm–Related Schemes for Conservation Laws. Technical Report MMU–9602, Department of Mathematics and Physics, Manchester Metropolitan University, UK, 1996.

[29] E. F. Toro. *Riemann Solvers and Numerical Methods for Fluid Dynamics, Second Edition.* Springer–Verlag, 1999.

[30] E. F. Toro and S. J. Billett. Centred TVD Schemes for Hyperbolic Conservation Laws. *IMA J. Numerical Analysis*, 20:47–79, 2000.

[31] E. F. Toro, R. C. Millington, and L. A. M. Nejad. Towards Very High–Order Godunov Schemes. In *Godunov Methods: Theory and Applications. Edited Review, E. F. Toro (Editor)*, pages 905–937. Kluwer Academic/Plenum Publishers, 2001.

[32] E. F. Toro, M. Spruce, and W. Speares. Restoration of the Contact Surface in the HLL–Riemann Solver. *Shock Waves*, 4:25–34, 1994.

[33] E. F. Toro and V. A. Titarev. Solution of the Generalised Riemann Problem for Advection-Reaction Equations. *Proc. Roy. Soc. London A*, 458:271–281, 2002.

[34] E. F. Toro and V. A. Titarev. TVD Fluxes for High-Order ADER Schemes. Technical Report NI03011-NPA, Isaac Newton Institute for Mathematical Sciences, University of Cambridge, UK, 2003.

[35] E. F. Toro (Editor). *Godunov Methods: Theory and Applications. Edited Review.* Kluwer Academic/Plenum Publishers, 2001.

[36] J. J. W. van der Vegt, van der Ven H., and O. J. Boelens. Discontinuous Galerkin Methods for Partial Differential Equations. In *Godunov Methods: Theory and Applications (Edited Review), E. F. Toro (Editor)*. Kluwer Academic/Plenum Publishers, 2001.

[37] B. van Leer. Towards the Ultimate Conservative Difference Scheme I. The Quest for Monotonicity. *Lecture Notes in Physics*, 18:163–168, 1973.

[38] B. van Leer. On the Relation Between the Upwind–Differencing Schemes of Godunov, Enguist–Osher and Roe. *SIAM J. Sci. Stat. Comput.*, 5(1):1–20, 1984.

[39] P. Woodward and P. Colella. The Numerical Simulation of Two–Dimensional Fluid Flow with Strong Shocks. *J. Comput. Phys.*, 54:115–173, 1984.

[40] H. C. Yee. Construction of Explicit and Implicit Symmetric TVD Schemes and their Applications. *J. Comput. Phys.*, 68:151–179, 1987.

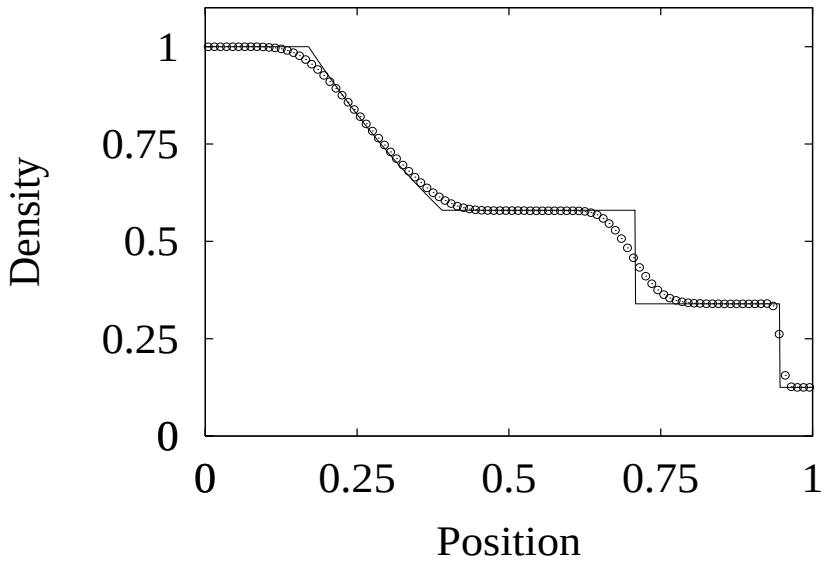

Figure 5: Test 1. Comparison for density between the exact solution (line) and the 3-stage $MUSTA_3$ scheme (symbol).

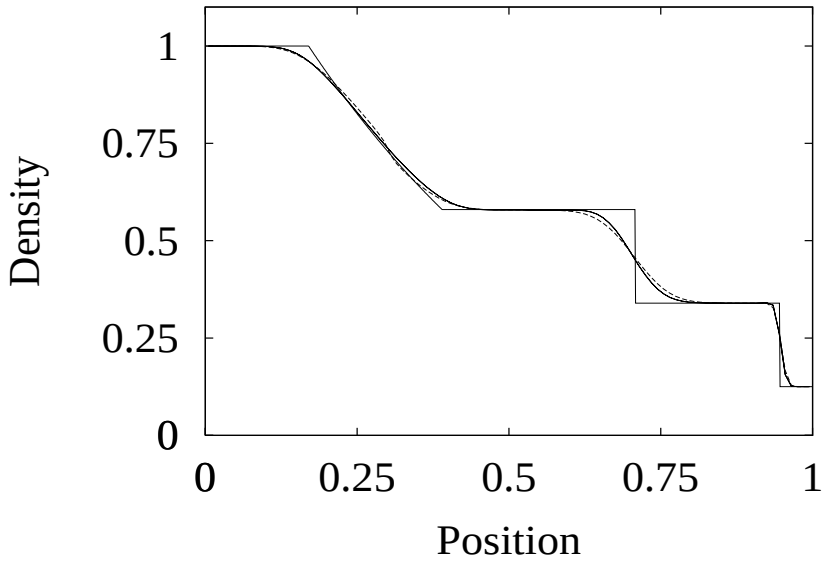

Figure 6: Test 1. Comparison for density between the exact solution (line), the Godunov method (dashed line) and the 3-stage $MUSTA_3$ scheme (full line).

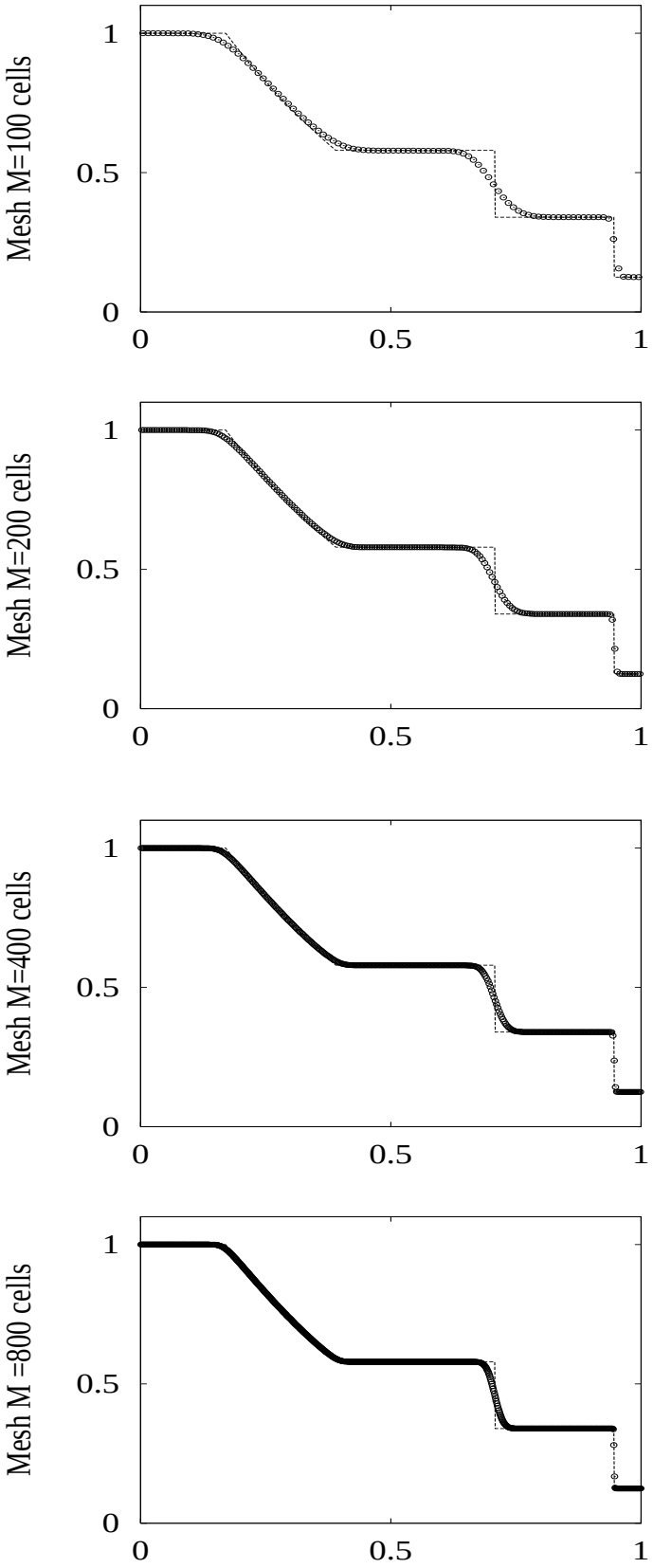

Figure 7: MUSTA scheme for Test 1. Numerical results for density (symbols) compared with the exact solution (line) for a sequence of four meshes.

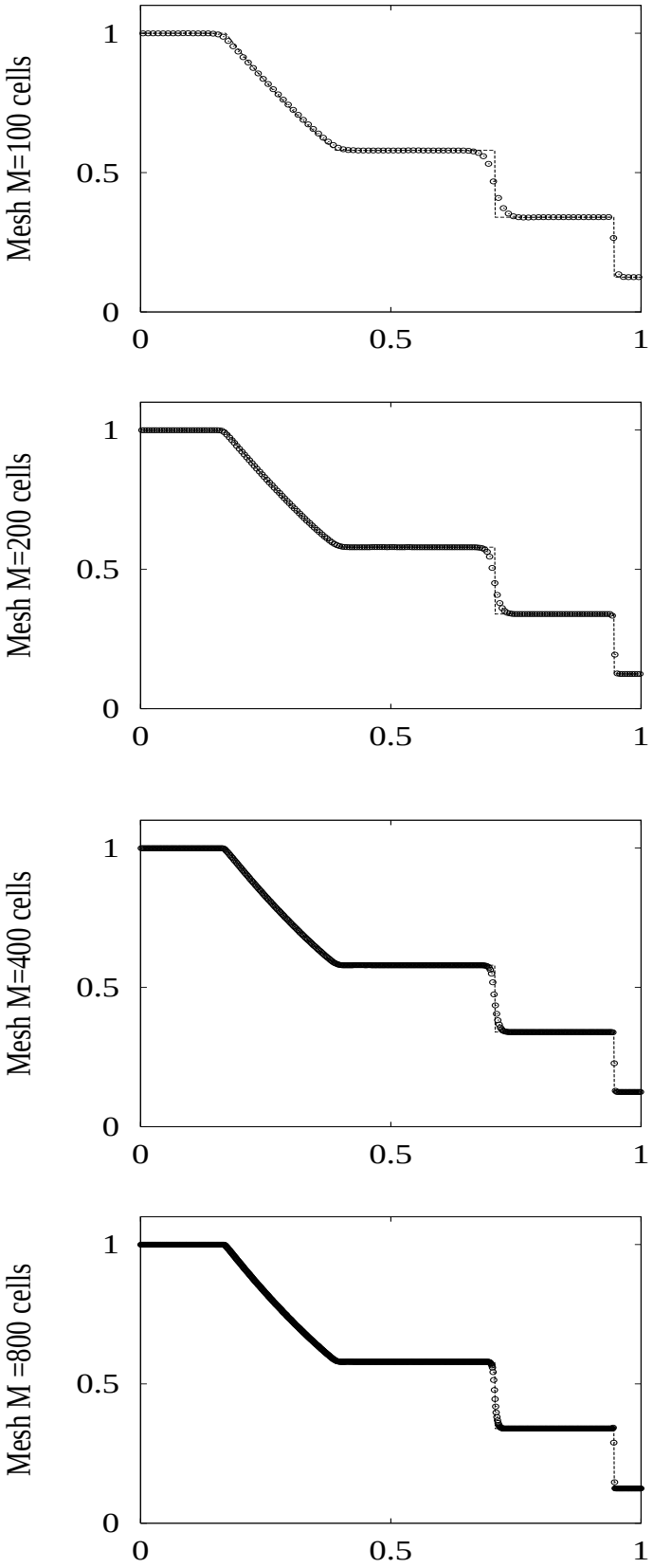

Figure 8: MUSTA TVD scheme for Test 1. Numerical results for density (symbols) compared with the exact solution (line) for a sequence of four meshes.

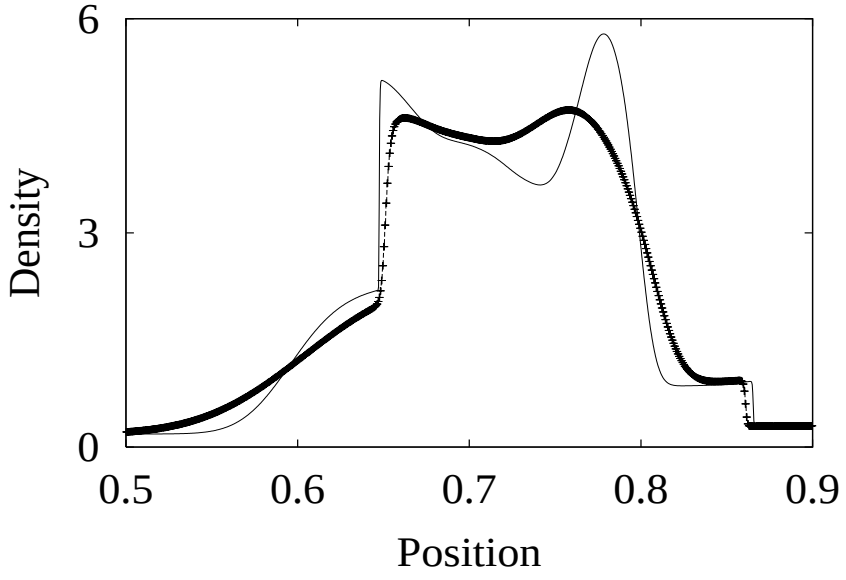

Figure 9: Comparison between the Godunov method (full line) and the Lax-Friedrichs scheme (symbols).

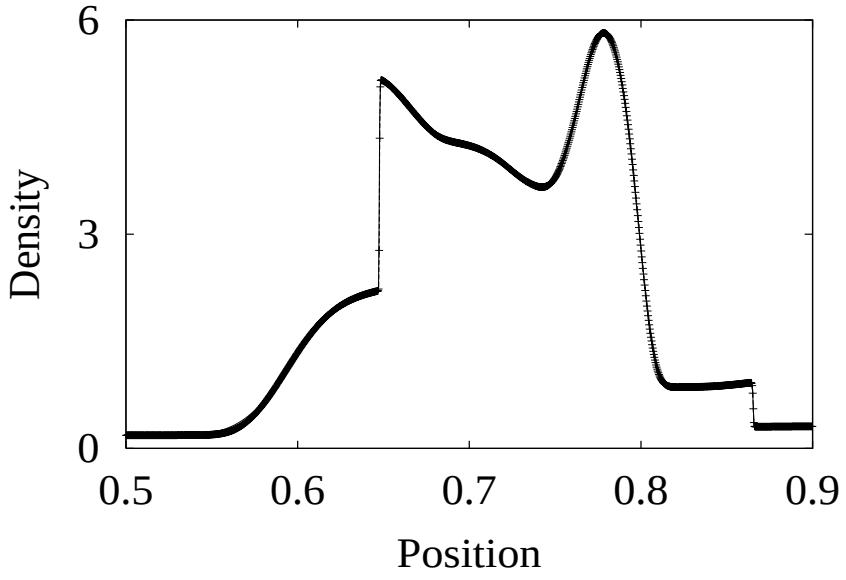

Figure 10: Comparison between the Godunov method (full line) and the 3-stage $MUSTA_3$ scheme (symbols).

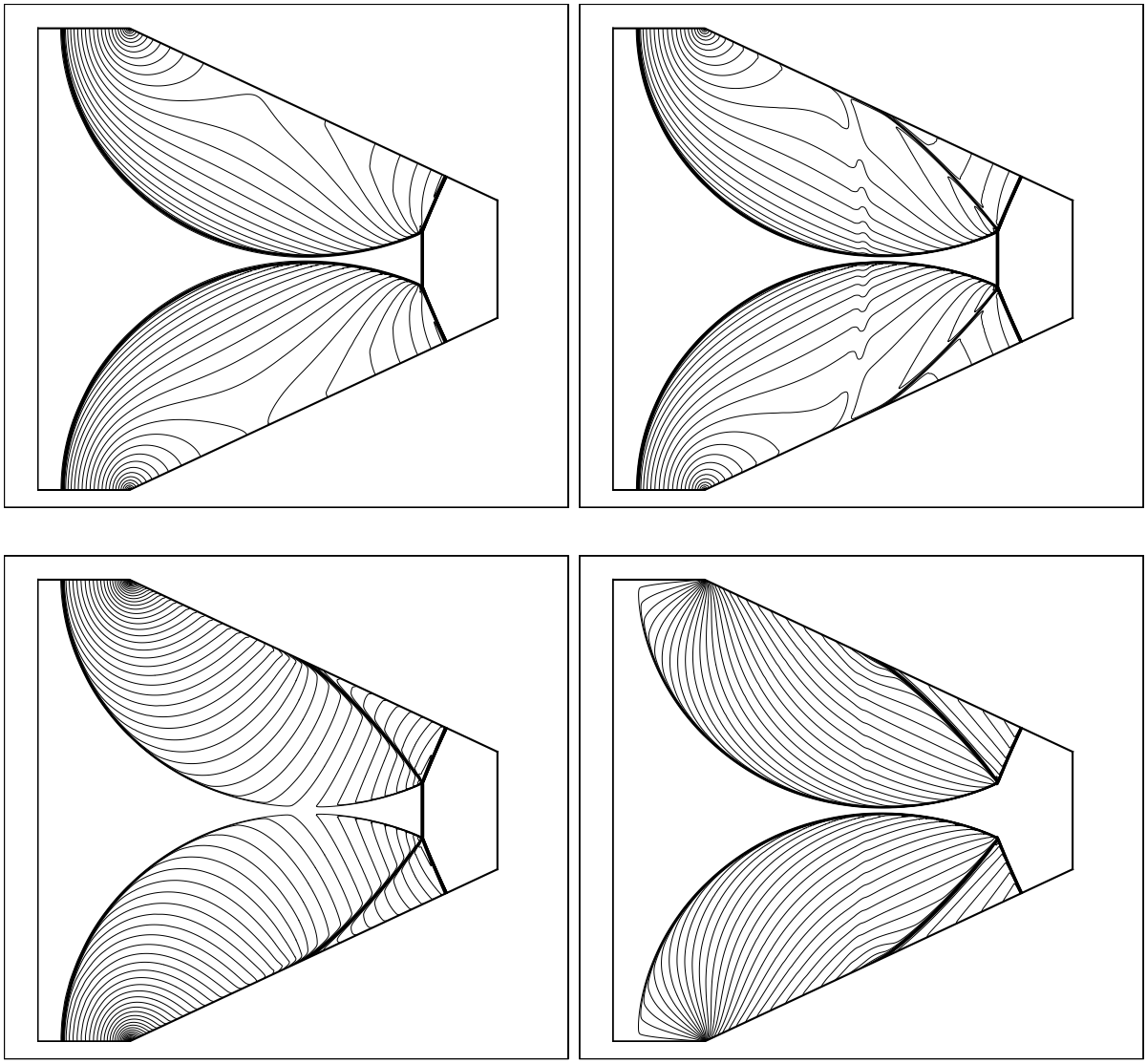

Figure 11: Test 3: Mach reflection problem. Numerical results at time $t = 1.0\ ms$ for mesh $M3 = 1000 \times 1000$ cells. Top row shows contours of pressure (left) and density (right); bottom row shows $x-$component of velocity (left) and $y-$component of velocity (right).

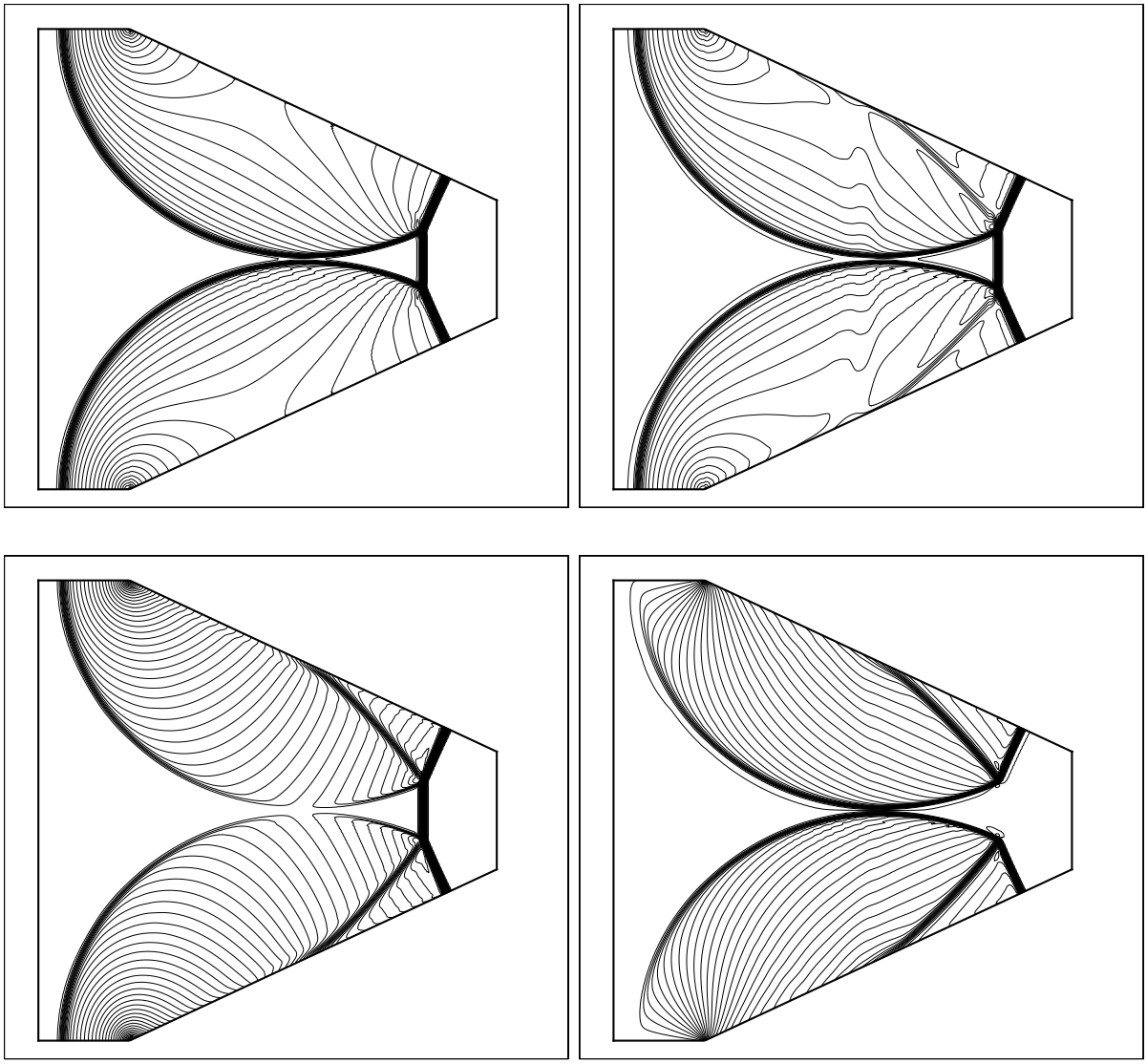

Figure 12: Test 3: Mach reflection problem. Numerical results at time $t = 1.0\ ms$ for mesh $M1 = 250 \times 250$ cells. Top row shows contours of pressure (left) and density (right); bottom row shows $x-$component of velocity (left) and $y-$component of velocity (right).

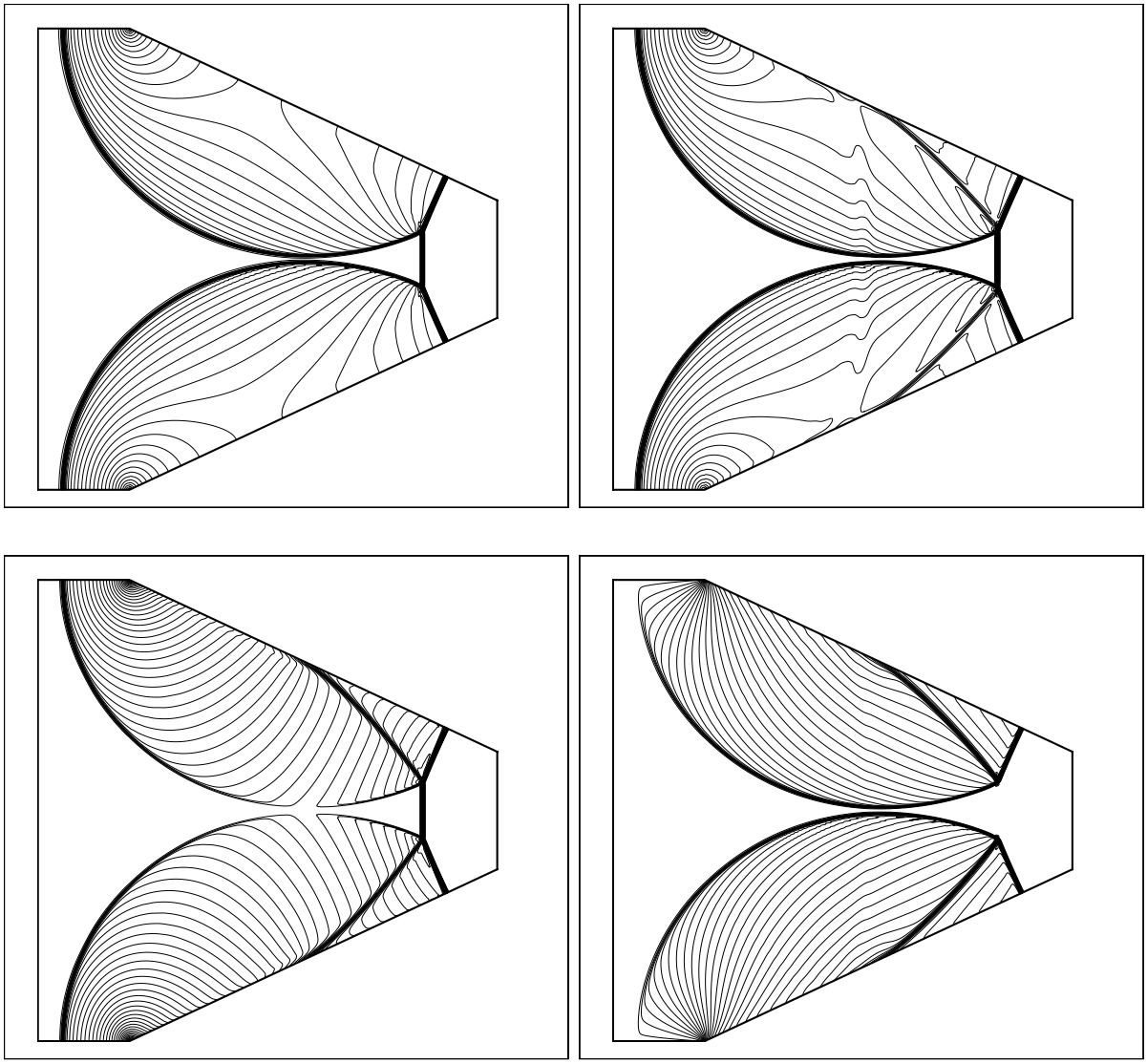

Figure 13: Test 3: Mach reflection problem. Numerical results at time $t = 1.0\ ms$ for mesh $M2 = 500 \times 500$ cells. Top row shows contours of pressure (left) and density (right); bottom row shows $x-$component of velocity (left) and $y-$component of velocity (right).

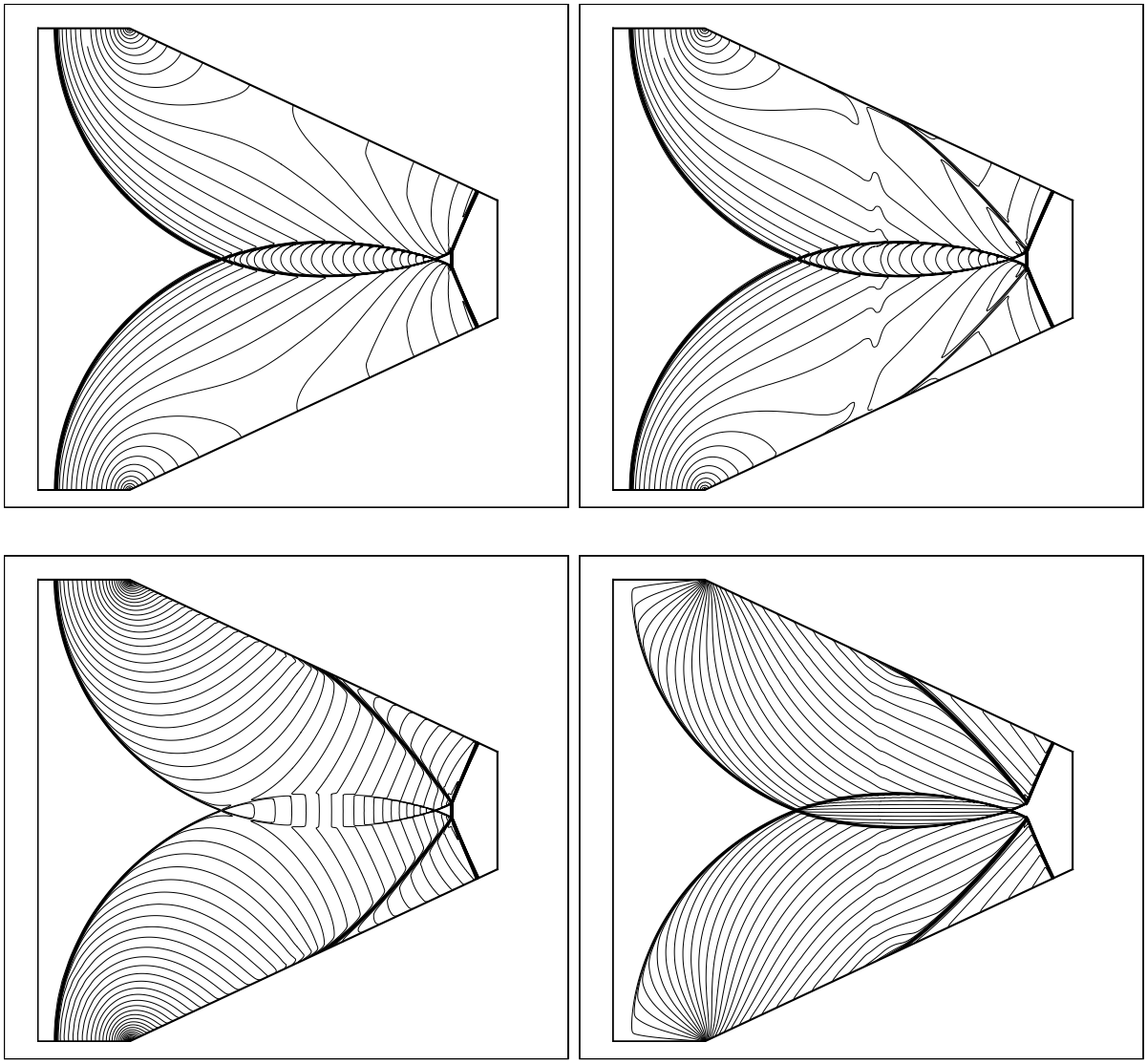

Figure 14: Test 3: Mach reflection problem. Numerical results at time $t = 1.1\ ms$ for mesh $M3 = 1000 \times 1000$ cells. Top row shows contours of pressure (left) and density (right); bottom row shows $x-$component of velocity (left) and $y-$component of velocity (right).